Article

pubs.acs.org/Biomac

High-Performance and Moisture-Stable Cellulose–Starch Nanocomposites Based on Bioinspired Core–Shell Nanofibers

Kasinee Prakobna,[†,‡] Sylvain Galland,[†,‡] and Lars A. Berglund*[,†,‡]

[†]Department of Fibre and Polymer Technology and [‡]Wallenberg Wood Science Centre, KTH Royal Institute of Technology, SE-10044 Stockholm, Sweden

Supporting Information

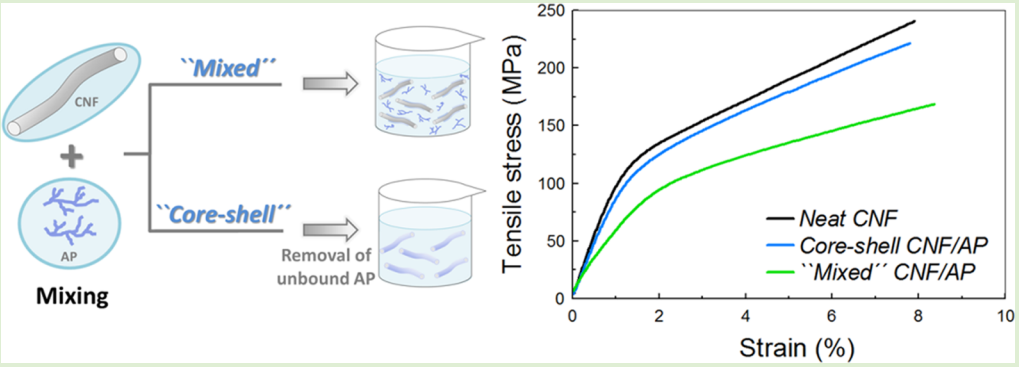

ABSTRACT: Moisture stability and brittleness are challenges for plant fiber biocomposites intended for load-bearing applications, for instance those based on an amylopectin-rich (AP) starch matrix. Core–shell amylopectin-coated cellulose nanofibers and nanocomposites are prepared to investigate effects from the distribution of AP matrix. The core–shell nanocomposites are compared with nanocomposites with more irregular amylopectin (AP) distribution. Colloidal properties (DLS), AP adsorption, nanofiber dimensions (atomic force microscopy), and nanocomposite structure (transmission electron microscopy) are analyzed. Tensile tests are performed at different moisture contents. The core–shell nanofibers result in exceptionally moisture stable, ductile, and strong nanocomposites, much superior to reference CNF/AP nanocomposites with more irregular AP distribution. The reduction in AP properties is less pronounced as the AP forms a favorable interphase around individual CNF nanofibers.

INTRODUCTION

Petroleum-based polymers tend to dominate load-bearing applications in engineering, packaging, and textiles products based on molded plastics and composites, polymer foams, plastic films, and fibers. In the long term perspective, a more sustainable approach is desirable where the polymers used are based on renewable resources such as plants. This would be a step toward reduced consumption of the limited resources of the planet earth. Narayan has discussed the concept of "materials carbon foot print",[1] where strong arguments are presented in favor of increased use of biobased plastics. Examples of biobased polymers include biopolyethylene and polylactides, where plant-based monomers are polymerized in industrial processes. Although the plant uses absorbed carbon dioxide from the atmosphere in the biosynthesis of starting compounds, considerable amounts of fossil-based energy are required during industrial synthesis of the final biopolymer. It is therefore of particular interest to investigate the potential of biological polymers such as cellulose, starch, and hemicelluloses.

Through biosynthesis, the plant performs polymerization of high molar mass polymers "for free" in water at ambient temperature and pressure. Cellulose is widely used in society since historical times due to its favorable physical properties, whereas the use of polymers such as hemicelluloses and amylopectin (AP) starch is limited by their poor hygromechanical properties. These native polysaccharides have heterogeneous molecular structure and composition and contain branches. The term "heteropolysaccharides" has been used in order to emphasize this characteristic.[2] After processing and drying, they are amorphous, glassy polymers of high glass transition temperature (T_g). They are usually very brittle and also sensitive to moisture, since their chemical and physical structure leads to high moisture sorption.

Cellulose in the form of wood products and plant fiber materials as well as chemical derivatives (films and fibers) is by far the most widely used biological polymer in load-bearing applications. Recently, cellulose nanofibers (CNF) disintegrated from wood has generated widespread interest.[3−5] After disintegration, CNF are readily available in the form of a dilute

Received: December 16, 2014
Revised: February 3, 2015
Published: February 4, 2015

DOI: 10.1021/bm5018194
Biomacromolecules 2015, 16, 904−912

hydrocolloid. The small size of this wood-derived component, with a diameter around 3−20 nm and a length of 0.7−3 μm, makes it possible to go beyond the materials structure limitations of wood and pulp fibers. CNF has been used to prepare novel nanostructured materials such as nanopaper,[6−8] foams,[9] polymer matrix composites,[10] aerogels,[11] inorganic hybrids,[12,13] and hydrogels.[14] The nanostructure and favorable mechanical performance of wood-based CNF networks in terms of modulus, ultimate strength and strain to failure[6] are important for the unique characteristics of these materials.

An interesting AP starch modification approach is to add CNF and prepare polymer matrix nanocomposites. The structures of the highly branched amylopectin component of starch and of CNF nanofibers are well-known and schematically illustrated in Figure S1. The AP consists of purely D-glucose residues on a glucan backbone but, in contrast to cellulose, AP has $\alpha(1 \rightarrow 4)$ glucan linkage along the main chain. It is one of the most commonly used biopolymers but has limitations in terms of hygromechanical properties. To improve mechanical, moisture barrier and film forming properties, nanocomposites based on CNF and AP can be prepared.[15−17] The improvement in physical properties of CNF/AP nanocomposites also depends on the dispersion of the nanofibers.[18,19] Composites based on cellulose microfibrils from potato tuber and a matrix of potato starch[20,21] (amylose and amylopectin) showed significantly reduced mechanical properties at elevated relative humidity (RH). Plasticized amylopectin/tunicin whisker composites[22] showed similar effects. Angles et al. conclude that poor interfacial adhesion between AP and cellulose is a problem in the system studied, where glycerol is added to lower T_g and improve ductility.[22] For wood based CNF/amylopectin,[17] it was suggested that water lowers interfacial adhesion more than glycerol plasticizer. The most plausible reason for this is the very high water solubility of AP.[23,24] Other studies of wood CNF and plasticized starch generally show quite low mechanical properties.[15,25] A typical moisture uptake of AP at ambient temperature and 50−60% RH is certainly above 10%.[26]

The present study is based on the hypothesis that poor nanostructural control contributes to the lack of favorable hygromechanical performance in CNF/starch composites. It means that there are local regions with CNF aggregates and regions where amylopectin starch forms matrix-rich pockets. CNF networks with aggregates of neat CNF are sensitive to moisture.[27] Local regions rich in starch would certainly be sensitive to moisture since T_g, yield stress and modulus would be reduced from plasticizing effects.

In contrast to man-made nanocomposites with heterogeneous matrix distribution, the primary plant cell wall contains heteropolysaccharides (hemicelluloses), which are distributed in a highly controlled manner. As the cellulose microfibrils are synthesized, hemicelluloses are adsorbed to the microfibrils.[28] The individual microfibril, with a diameter of 3−4 nm, is thus coated by hemicellulose, forming a "core-shell" nanofiber. Interestingly, the primary plant cell wall is highly hydrated and yet demonstrates good mechanical function.[29] One reason is physical cross-linking so that hemicellulose molecules form physical links between the microfibrils.[29,30] The adsorption of hemicellulose to microfibrils also takes place in the secondary cell wall[31] and is an elegant way to control the nanostructure. The hemicellulose coating moderates the properties of the cell wall, prevents microfibril agglomeration and contributes to the mechanical cell wall stability in moist state (facilitates physical cross-linking).

Previous studies on polymer-coated cellulose nanofibers include bacterial cellulose coated by hydroxyl ethyl cellulose (HEC),[32] and wood CNF coated by HEC.[7,33] It has also been suggested that preadsorption of a soft polymer to nanofibrillated cellulose (CNF) could result in nanofibers useful as a paper strength additive in papermaking.[34] A recent attempt to coat wood CNF with hemicelluloses was unsuccessful in terms of improved property characteristics, although the reasons for lack of observable effects were not clarified.[35]

In the present study, effects from nanoscale distribution and interphase formation of an AP polymer matrix are investigated with respect to hygromechanical properties of CNF/AP nanocomposites. Core−shell CNF inspired by primary plant cell wall structures are used in nanocomposites prepared by filtration, without loss of polymer matrix. Nanostructure and hygromechanical properties are compared with CNF/AP nanocomposites obtained from conventional mixing of the two constituents and where the material components are less well distributed.

EXPERIMENTAL SECTION

Material. The enzymatic CNF suspension was prepared from spruce sulphite pulp (Nordic Pulp and Paper, Sweden), containing 13.8% hemicelluloses and 0.7% lignin. The pulp was first subjected to pretreatment steps including enzymatic degradation and mechanical beating according to a previously reported method.[36] Subsequently, the pretreated pulp was disintegrated by passing through a Microfluidizer (Microfluidics Ind., U.S.A.) for three times with big chambers (diameter of 400 and 200 μm), and then five times with small chambers (diameter of 200 and 100 μm). The pretreated pulp fibers were fibrillated down to nanoscale. A 2 wt % stable CNF suspension in water was successfully prepared. The obtained CNF has hemicelluloses content of 12.3 wt % and degree of polymerization (DP) of 1550. The DP was determined from intrinsic viscosity using a procedure similar to that previously described.[36]

Maize amylopectin (AP) was purchased from Sigma-Aldrich (GmbH, Germany). The preparation of an amylopectin solution was adapted from previous study.[37] An aqueous suspension of 1 wt % amylopectin was prepared with deionized (DI) water. This AP suspension was heated and held at 65 °C for 5 min with magnetic stirring for pregelatinization. Then it was heated to 135 °C for another 2 h in an oil bath, while the concentration of AP was kept at 1 wt % during preparation. The obtained AP solution showed optical transparency. The degree of polymerization (DP) of neat AP and its branched chain are 1.03×10^6 and 37.4, respectively; see SI (Table S1).

Adsorption of AP on CNF. The warm AP solution (1 wt %) was introduced to the CNF suspension (2 wt %) in order to obtain a series of CNF/AP weight ratio of 1:0.1, 1:0.25, 1:0.5, 1:1, and 1:2, which corresponds to AP fraction of 10−70 wt %. The aqueous mixtures of CNF and warm AP (temperature 135 °C) were mixed at room temperature with magnetic stirring for 24 h to ensure equilibrium adsorption, see SI (Figure S2). Then they were subjected to centrifugation at a speed of 4500 rpm for 10 min, and the supernatants containing unbound AP were removed. The samples were washed carefully and subjected to centrifugation for another three times. The bottom phase containing cellulose nanofibrils coated with adsorbed AP was collected for further adsorption measurement and preparation of Core−shell CNF/AP nanocomposite films.

Preparation of CNF Nanopaper. The 2 wt % CNF suspension was diluted with DI water to the final concentration of 0.2 wt %, and mixed at 8000 rpm using an Ultra Turrax mixer (IKA, T25 Digital) for 3 min. The sample was degassed for 10 min, and then vacuum filtered on a glass filter funnel using a 0.65 μm filter membrane (DVPP, Millipore), according to the previously reported method for

DOI: 10.1021/bm5018194
Biomacromolecules 2015, 16, 904−912

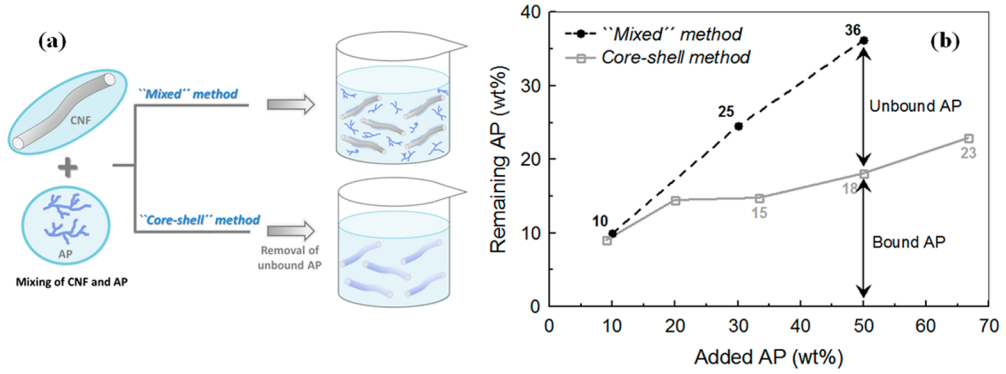

Figure 1. (a) Sketch illustrating the two different preparation methods, which result in "Mixed" CNF/AP and "Core–shell" CNF/AP nanocomposites. (b) Remaining amount of AP (remaining AP) in the CNF/AP nanocomposites determined by sugar analysis. AP contents in the nanocomposite films are represented next to the corresponding data points. In case of the core–shell nanocomposites, the three samples with highest AP fractions were selected for nanocomposite preparation.

nanopaper.[6] The wet cake of CNF was formed after filtration. To prepared CNF nanopaper, the wet cake was dried using a laboratory sheet dryer (Rapid Köthen) at 93 °C under vacuum of about 70 mbar for 10 min.[12] The nanopaper prepared from CNF exhibited crystallinity of 58%, see SI (Table S2).

Preparation of Core–Shell CNF/AP Nanocomposite Films. The nanocomposite of CNF coated with adsorbed AP is referred to as Core–shell CNF/AP. The mixtures of CNF and AP with CNF/AP weight ratios of 1:0.5, 1:1, and 1:2 were selected for film preparation. To prepare the nanocomposite films, they were subjected to mixing, degassing, filtration and drying, as described above for CNF nanopaper. The AP fractions adsorbed on CNF were determined by sugar analysis. The corresponding AP contents in the nanocomposite films were 15, 18, and 23 wt %, respectively.

Preparation of "Mixed" CNF/AP Nanocomposite Films. The mixtures of CNF/AP with AP fractions of 10, 30, and 50 wt % were prepared from AP solution (1 wt %) and CNF suspension (2 wt %). The obtained mixtures were adjusted to a final concentration of 0.2 wt % CNF with warm DI water (temperature 90 °C). The samples were carefully mixed and subjected to film formation, similar to as described above in Core–shell CNF/AP nanocomposite films. However, the step of unbound AP removal after mixing was neglected. Some fraction of unbound AP still remains. The AP matrix content in the "Mixed" nanocomposites were determined by sugar analysis, and the corresponding data were 10, 25, and 36 wt %.

Preparation of AP Films. AP film was prepared from the aqueous solution of 1 wt % AP by solvent casting. The solution was carefully casted on polystyrene Petri dishes coated with Teflon. The AP film was peeled off from the mold after drying at 40 °C in oven for 3 days. The thickness of the resulting films was approximately 30–40 μm.

Sugar Analysis. To characterize the AP matrix in the nanocomposites, freeze-dried sample of CNF and CNF/AP nanocomposites were subjected to acid hydrolysis. Their sugar compositions were quantitatively determined by high-performance anion exchange chromatography with pulsed amperometric detection (HPAEC-PAD) based on SCAN-CM71:09. The HPAEC-PAD was connected with a CarboPac PA-1 column. Data was processed with Chromeleon software. The difference in percentage of glucose content between pure CNF and CNF/AP samples allows the data to be calculated and expressed as amount of AP in the nanocomposite films.

Dynamic Light Scattering (DLS). DLS measurements were performed using a Zetasizer Nano ZEN3600 (Malvern Instruments Ltd., U.K.). The suspensions of Neat CNF and Core–shell CNF/AP were diluted to a final concentration of 100 mg/L. They were filtered through 5 μm membrane (Acrodisc) and then filled in PMMA cuvettes. All measurements were performed at 25 °C. The results were reported based on an average of at least three measurement data.

Atomic Force Microscopy (AFM). A diluted suspension of Neat CNF and Core–shell CNF/AP was spin-coated on a mica disc (Ted Pella Inc., U.S.A.). The AFM experiment was conducted using a multimode Nanoscope IIIa AFM (Veeco Ltd., U.S.A.). Images were acquired in tapping mode in air using a silicon cantilever (Bruker, U.K.). The drive frequency of the cantilever was approximately 150 kHz. The cantilever had a tip radius of 8 nm and spring constant of 5 N/m. The height images were reported and 150 nanofibrils were analyzed for width distribution of nanofibrils in each sample.

Dynamic Vapor Sorption (DVS). Moisture sorption measurements were made with DVS (Surface Measurement Systems Limited, U.K.). A sample of up to 20 mg was placed in the sample cup and then weighed with a resolution of 0.1 μg. The experiments were conducted at 32 °C with relative humidities (RH) setting to 0, 20, 40, 60, 80, and 90 RH%. A time of approximately 400 min was used at each step to ensure steady-state condition. The DVS sorption isotherm was calculated from an average of the last 20 min in each RH-step. The moisture uptake was calculated based on a single measurement according to the equation:

$$\text{moisture uptake} = 100 \times \frac{W_{\text{moist}} - W_{\text{dry}}}{W_{\text{dry}}}$$

where W_{moist} is the sample weight equilibrated at certain RH% and W_{dry} is the dry weight of the sample at 0 RH%.

Tensile Tests. The mechanical properties of CNF, AP, and all CNF/AP nanocomposite films at humidity conditions of 50 and 85 RH% were examined. All samples were conditioned at 23 °C under controlled RH for at least 1 week. Tensile testing was performed on an Instron 5944 equipped with a 500 N load cell. The gauge length was adjusted to 20 mm. The specimens were cut into a rectangular strip with width dimension of 5 mm. The stress–strain curves of all specimens were recorded at a strain rate of 10% min^{-1}. The tensile properties of each sample were reported based on an average value of at least five specimens.

To obtain accurate value of Young's modulus, the grip displacement was corrected by Digital Speckle Photography (DSP) calibration. In order to monitor strain, a fine pattern of black dots was sprayed on the surface of specimens. Strain values were analyzed using Vic 2D Software. A correlation of strains determined from the DSP and the grip displacement was established. The reported modulus is the corrected value obtained from DSP calibration.

Field-Emission Scanning Electron Microscopy (FE-SEM). Fracture surface of film samples, which were freeze-fractured under liquid N_2, was examined with a Hitachi S-4800 scanning electron microscope. The samples were mounted on a metal stub, and then coated with graphite and gold–palladium using Agar HR sputter coater for 5 and 30 s, respectively. The acceleration voltage was set in the range of 1–2 kV.

Transmission Electron Microscopy (TEM). The CNF/AP nanocomposite films with AP content of 23–25 wt % were embedded in an epoxy resin prior to the cutting process at room temperature. The cross-sectioning was carried out using an ultramicrotome (Leica

DOI: 10.1021/bm5018194
Biomacromolecules 2015, 16, 904–912

EM UC7, Germany) equipped with a diamond knife (DiATOME, Switzerland). The ultrathin specimens were collected on TEM copper grids (PELCO 1GC400, TedPella, USA), and stained by exposure for 1 h to RuO_4 vapors. The samples were observed by TEM (FEI Tecnai Spirit, U.S.A.).

RESULTS AND DISCUSSION

Preparation of CNF/AP Nanocomposites with Different Polymer Matrix Distributions. CNF/AP nanocomposites were prepared by two different methods, see Figure 1a. A colloidal CNF suspension was mixed with an AP solution according to the procedure in the experimental section. In the simpler "Mixed" method, the CNF/AP mixture is directly subjected to filtration and drying so that a solid CNF/AP nanocomposite is formed, termed "Mixed" CNF/AP. Most of the AP polymer is trapped in the CNF network, although some AP will be lost during filtration. Due to the nature of this preparation method, it is expected that AP will be unevenly distributed in "Mixed" CNF/AP, at least at the nanoscale.

In the second Core−shell method, the excess AP still in solution is removed from the colloidal CNF/AP mixture by several centrifugation/washing steps. The purpose is to remove "unbound" AP, which is dissolved in the water phase (see "Removal of unbound AP" in Figure 1a). For the Core−shell method it is therefore expected that AP is present only as an associated or adsorbed AP shell coating of the CNF core nanofibers. The core−shell CNF/AP is processed as a colloid and subjected to filtration and drying so that a solid nanocomposite film is formed, termed Core−shell CNF/AP. The nanofibers on which Core−shell CNF/AP nanocomposites are based are not expected to lose any AP polymer during filtration.

The nanocomposites prepared by the two different preparation methods were compared with respect to AP content in the final nanocomposite film. The AP content was estimated from sugar analysis, as described in the Experimental Section. Data are presented in the form of AP content in the final material (remaining AP) as a function of added AP content in the aqueous CNF/AP mixture (added AP), see Figure 1b. The lower curve (Core−shell method) results in 15−23 wt % AP in the solid CNF/AP nanocomposite as 20−65 wt % of AP is added. For instance, as 50 wt % AP is added, 18 wt % remains in the solid nanocomposite after centrifugation, washing, and drying.

In contrast to the Core−shell method, the "Mixed" method results in twice as much AP in the solid nanocomposite (36 wt % AP). This is interpreted in terms of the concepts Bound AP and Unbound AP. For the Core−shell method, the AP is strongly associated or adsorbed to CNF. The term Bound AP is therefore used to describe the AP. The term is simply defined as the amount of AP remaining after centrifugation and washing. Since Bound AP molecules are physically adsorbed, one may expect that the molecular mobility of the AP is reduced by its confinement to the CNF surface. For the "Mixed" method, a larger amount of AP is present in the solid nanocomposite, see the upper curve in Figure 1b. From the total 36 wt %, half of it, 18 wt %, is Bound AP and another 18 wt % is assumed to be Unbound AP. The term Unbound AP is just defined as the "extra" AP trapped in the nanocomposite due to the nature of the preparation method. Unbound AP is likely to have properties related to those of AP molecules in bulk form.

From a practical point of view, one may note that as 10 wt % AP is added, virtually all AP is adsorbed so that Core−shell CNF/AP nanofibers are formed. For this composition, no centrifugation is needed and all AP is assumed to form a shell coating. Note that the "Mixed" method is carefully performed with favorable conditions in terms of well-dispersed CNF, high AP solubility in water and long mixing time. However, the amount of AP after filtration, and its distribution in the nanocomposite structure, will depend on processing conditions since a substantial AP fraction is trapped rather than adsorbed in the CNF/AP network. In contrast, the Core−shell method involves filtration without any polymer loss. Also, the distribution of the polymer matrix is controlled prior to filtration.

Size Distribution of Neat CNF Nanofibers and Core−Shell CNF/AP Nanofibers. The colloidal behavior of CNF nanofibers is important for the nanocomposite structure in the dried CNF/AP film. Well-dispersed nanofibers in colloid can be obtained due to repulsion forces between nanoparticles based on either electrostatic or steric hindrance,[38] so that the extent of agglomeration is limited. Previous authors have adsorbed small amounts (1−2 wt %) of nonionic polymers to CNF in suspension.[39−41] This reduced the amount of large CNF aggregates, probably through steric hindrance effects. Strength and strain to failure of dried films was then improved, possibly because of reduced aggregate size.

The size distributions of Neat CNF and Core−shell CNF/AP nanofiber colloids are presented in Figure 2. The results

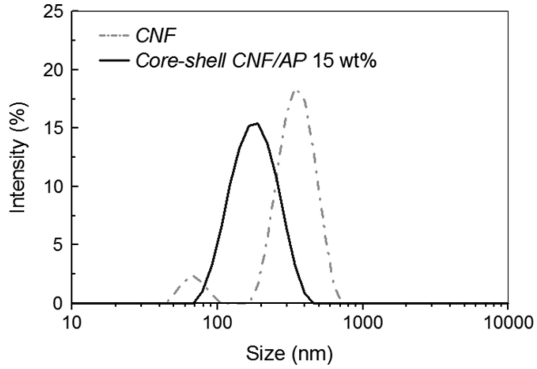

Figure 2. Estimated size distributions of neat CNF nanofibrils and Core−shell CNF/AP 15 wt % nanofibrils in aqueous suspension based on DLS data (dynamic light scattering). Note that the reported size distribution is based on an assumption of spherical particles, which is not the true geometry of CNF.

show that Neat CNF displays a bimodal size distribution with average diameters at 68 and 361 nm. Instead, Core−shell CNF/AP reveals a fairly broad unimodal distribution with an average diameter of 186 nm. The larger aggregates (361 nm) are absent in Core−shell CNF/AP. The origin of the 186 nm peak is unclear, but could possibly be due to association of small particles. It is encouraging that CNF and AP can be mixed without flocculation or precipitation phenomena. Both suspensions were stable. The lower average particle size for Core−shell CNF/AP indicates a lower fraction of aggregates. The adsorbed AP alters particle−particle interaction, probably due to steric hindrance. The polymer chain conformations determine the steric stabilization mechanisms.[42] The present results suggest that Core−shell CNF/AP colloids offer promise for preparation of well-dispersed nanocomposites with fairly

DOI: 10.1021/bm5018194
Biomacromolecules 2015, 16, 904−912

high amounts of associated AP with the CNF. The branches present on AP molecules may have positive effects.

Nanostructure of Neat CNF Nanofibers and Core–Shell CNF/AP Nanofibers. The diameters of Neat CNF and Core–shell CNF/AP nanofibers were measured by AFM in tapping mode. The height distributions of both types of nanofibers show that 86–87% of the populations have a lateral dimension in the range of 0–10 nm (Figure 3 and Table 1).

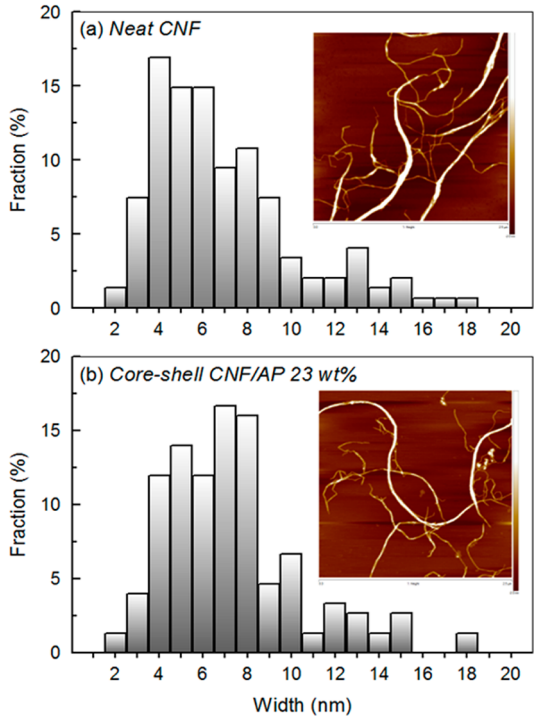

Figure 3. Height distributions of (a) Neat CNF nanofibers and (b) Core–shell CNF/AP nanofibers containing 23 wt % AP. The inset of AFM images with the scan size of 2.5 × 2.5 μm is presented. The vertical scale bar at the right edges of the insets represents height, where the length of the scale bar is 14 nm and the most light-colored region (white) has the largest height.

The number-average value d_n is 6.6 and 7.0 nm for Neat CNF and Core–shell CNF/AP, whereas the weight-average d_w is 8.4 and 8.6 nm. The polydispersity index is as low as 1.3 and 1.2, respectively. The larger diameter for Core–shell CNF/AP is in support of a core–shell nanofiber structure, although the difference is smaller than expected (approximately 1 nm difference in size for 6 nm nanofibers) and not statistically significant. However, if only the range 3–8 nm is considered, the difference in diameter is substantial. In the more narrow range 3–8 nm, the corresponding fractions are 74–75%. Neat CNF has the majority of this fraction in the 3–5 nm range, whereas Core–shell CNF/AP has a very strong majority of its nanofibers in the 6–8 nm range, see Table 1.

AFM images of the nanofibers (insets in Figure 3) show both aggregated nanofiber bundles and individual fibrils of small diameter. Branched structures are apparent. They are nanofiber aggregates where individual nanofibers form the branches. Aggregates are typically longer than individual fibrils and can extend several micrometers. Nanofibers show curved segments and kinks, rather than straight rod-like sections. This indicates the presence of localized defects, probably formed during mechanical disintegration from the pulp fibers. Most likely, the CNF have limited bending stiffness and substantial flexibility.

Structure of "Mixed" CNF/AP and Core–Shell CNF/AP Nanocomposites. In order to characterize the nanostructure of the materials, the two nanocomposite samples were subjected to low temperature freezing followed by manual cutting to induce brittle fracture. The fracture surfaces were observed by FE-SEM, see Figure 4a,b. A lamellar structure is

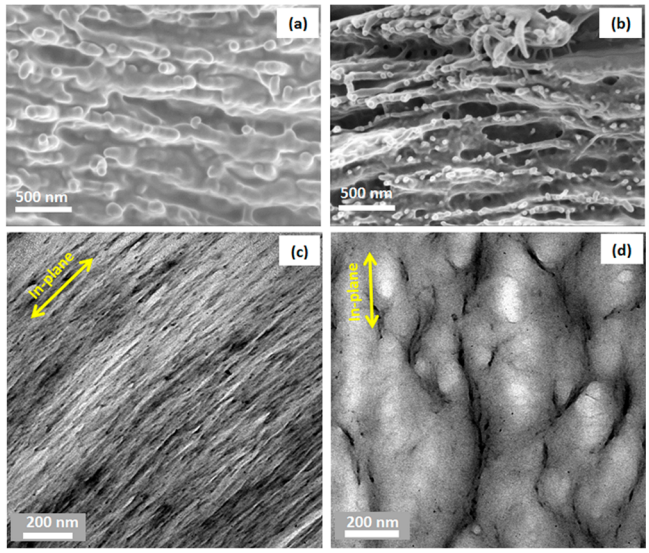

Figure 4. High magnification FE-SEM images of liquid nitrogen freeze-fractured surfaces of nanocomposites: (a) Core–shell CNF/AP 23 wt % and (b) "Mixed" CNF/AP 25 wt %; and TEM images of nanocomposites: (c) Core–shell CNF/AP 23 wt % and (d) "Mixed" CNF/AP 25 wt %.

observed in both materials, as has been reported for CNF films[6] and CNF/AP-rich nanocomposites.[17] In SI, Figure S4 shows distinct lamellar structure also in Neat CNF films. This may be related to the formation of "flocs" as the concentration of CNF becomes very high during filtration, in the local region close to the filtering membrane.

Based on the adsorption data in Figure 1b and the diameter data in Table 1, we propose the Core–shell CNF/AP to consist

Table 1. Number Average and Weight Average Diameter (d_n and d_w) and % Fraction of Neat CNF and Core–Shell CNF/AP Nanofibers in Different Ranges of Diameters[a]

	all nanofibers			fraction of 0–10 nm						
							% fraction of all nanofibers (nm)			
sample	d_n	d_w	PDI	d_n	d_w	PDI	2.5–5.5	5.5–8.5	8.5–10.5	0–10
Neat CNF	6.6 ± 3.3	8.4	1.3	5.7 ± 2.2	6.3	1.1	39.2	35.1	10.8	86.5
Core–shell CNF/AP 23 wt %	7.0 ± 3.2	8.6	1.2	6.1 ± 2.0	6.6	1.1	30.0	44.7	11.3	87.3

[a]The data is based on analysis of AFM height images.

DOI: 10.1021/bm5018194
Biomacromolecules 2015, 16, 904–912

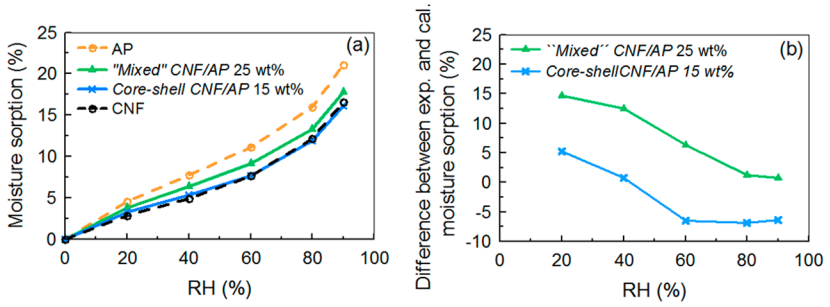

Figure 5. Dynamic vapor sorption data showing (a) isotherms of solid films based on Neat AP, "Mixed" CNF/AP, Core−shell CNF/AP, and Neat CNF at 32 °C, and (b) difference between experimental data and calculated values (rule of mixtures) of moisture sorption for "Mixed" CNF/AP and Core−shell CNF/AP nanocomposites. Negative value means that the material adsorbs less moisture than predicted from rule of mixtures.

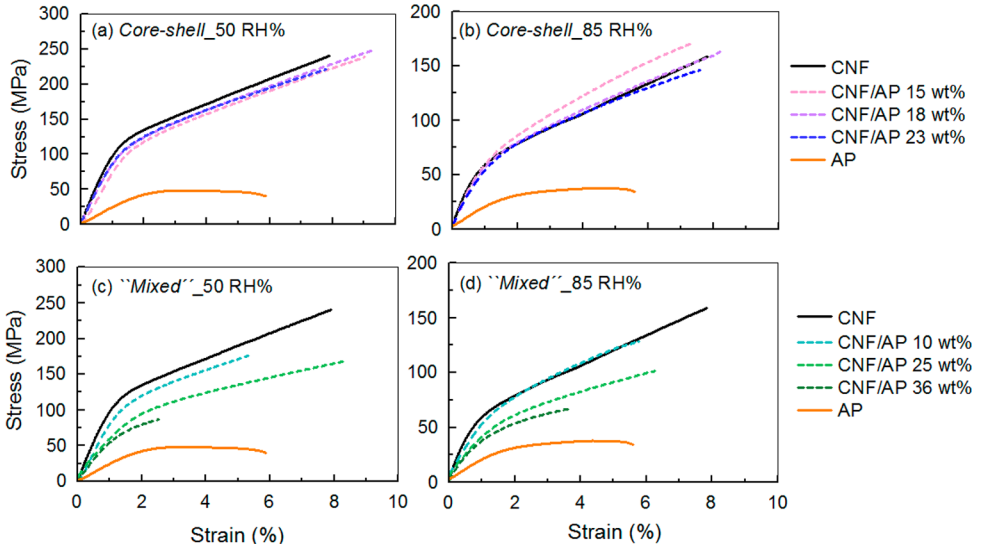

Figure 6. Tensile stress−strain curves of CNF, AP, and their nanocomposites of (a, b) Core−shell CNF/AP and (c, d) "Mixed" CNF/AP under testing condition of 50 RH% and 85 RH%, respectively.

of CNF nanofibers coated by a layer of AP. In Figure 4a, the Core−shell CNF/AP nanocomposite shows comparably large diameter (>50 nm), diffuse fibrous entities whereas no individual CNF nanofibers are apparent at the expected scale of 10 nm. In contrast, small diameter CNF nanofibers are observable in the "Mixed" CNF/AP material in Figure 4b. The AP matrix distribution appears homogeneous in Core−shell CNF/AP, but is inhomogeneous in "Mixed" CNF/AP. In Figure 4b, the "Mixed" CNF/AP appears to show AP-rich layers between CNF-rich laminae. Also, the thickness of individual lamina is much larger for Core−shell CNF/AP than for "Mixed" CNF/AP.

TEM of thin cross sections was performed to assess the structure. The difference betweeen the fine structure in Figure 4c, Core−shell CNF/AP, and the coarser structure in Figure 4d, "Mixed" CNF/AP is apparent. The Core−shell CNF/AP is organized at a very fine scale, with fibrous entities at the scale of 10 nm (but also larger and smaller). They form a layered structure, consistent with Figure 4a, although at finer scale. The image is from a cut section, so the differences between light and dark regions may be influenced by thickness differences. Since the CNF are random-in-the-plane, a cross-section means that CNF nanofibers are cut by the ultramicrotome knife. It is possible that the small-scale dark dots are due to individual CNF nanofibers. Since many of the fibrous entities are larger than the diameter of individual CNF's, the Core−shell CNF/AP may contain CNF/AP nanofibers organized as parallel fibrous agglomerates.

The structure of "Mixed" CNF/AP at this scale is much more coarse, see Figure 4d. Although CNF cellulose has higher density than AP, this difference may not be sufficient for contrast. Light areas are consistent with regions of some porosity (low density), whereas dark regions may be regions rich in CNF-aggregates. Images at the 1 μm scale (see SI, Figure S5) show that staining cross sections of "Mixed" CNF/AP consist of agglomerated CNF "flocs" with AP-rich regions in between.

The preparation scheme, AP adsorption data to CNF, and AFM and TEM observations are consistent with a structure in Core−shell CNF/AP corresponding to the schematic model in SI (Figure S6). Individual core−shell nanofibers form bundles of parallel, individual CNF/AP nanofibers. Those bundles form random-in-the-plane layers, which are thinner and more homogeneous in structure and contains better dispersed CNF's compared with "Mixed" CNF/AP.

Moisture Sorption. Starch-based polymers such as AP tend to be hygroscopic and mechanical properties decrease substantially due to moisture sorption. Dynamic vapor sorption (DVS) measurements were therefore performed. Figure 5a shows moisture sorption isotherms for Neat CNF, Neat AP, and CNF/AP nanocomposites films, where the nanocomposites are prepared by Core−shell and "Mixed" methods.

DOI: 10.1021/bm5018194
Biomacromolecules 2015, 16, 904−912

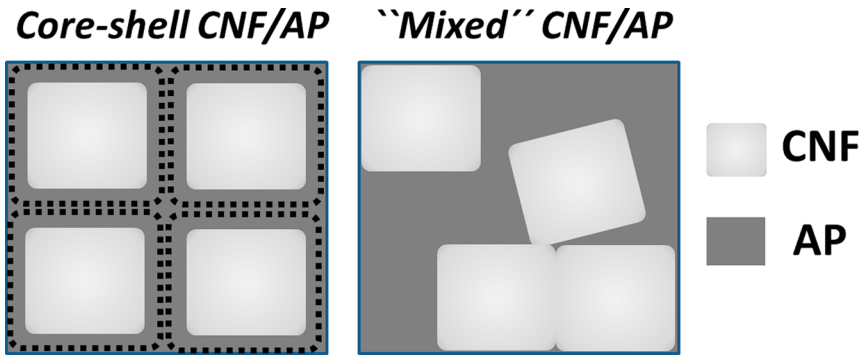

Figure 7. Illustration of local polymer matrix distribution in Core−shell CNF/AP and "Mixed" CNF/AP nanocomposites. The dashed line indicates the boundary between the coated AP layer on the CNF surface in Core−shell nanocomposites.

All curves classify into type II isotherms, indicating multilayer adsorption after completion of a single monolayer of sorbed vapor.[43] All isotherms displayed a first inflection at 20 RH% assigned to the initiation of multilayer sorption, and the second inflection appears to take place at 60 RH%. The mechanism controlling upward bend in the second inflection has been described as softening of amorphous polymers.[44] At this transition, the material is more susceptible to water molecules as the molecular interaction of nanocomposite consitituents become less favorable. As expected, the Neat AP film exhibited highest sorption. The moisture content then decreased as CNF content was increased.

The Core−shell CNF/AP 15 wt % shows very low moisture sorption, which is even comparable to the Neat CNF film. The comparison between predictions and experimental data in Figure 5b makes it possible to compare two compositions with different AP content. At higher RH, the Core−shell CNF/AP 15 wt % adsorbs less moisture than rule of mixtures predictions based on data for Neat CNF and Neat AP components, see Figure 5b and SI (Table S3). This is not the case for "Mixed" CNF/AP. Most likely, there are fewer available sites for moisture sorption in Core−shell CNF/AP. Strong interfacial interaction at the molecular scale between the CNF surface and associated AP may reduce the accessibility of hygroscopic AP sites. AP closely associated with CNF is also expected to have very different molecular conformations compared with bulk AP, with less free volume.

The "Mixed" CNF/AP 25 wt % exhibited higher moisture sorption compared with expected value based on the rule of mixture, see Figure 5b and SI (Table S3). Possibly, there is a contribution from the porosity in "Mixed" CNF/AP, see SI (Table S4).

Mechanical Properties in Tension. A comparative study of tensile properties of CNF/AP nanocomposites of different AP content conditioned at different relative humidities was carried out, see Figure 6 and the corresponding data in SI (Tables S4 and S5). The main purpose was to compare effects from the difference in polymer matrix distribution between "Mixed" CNF/AP and Core−shell CNF/AP. The Neat CNF and Neat AP materials were included to provide reference values for nanofiber network and polymer matrix properties.

The pure AP film in our study was successfully prepared in the absence of plasticizer. In previous work, a plasticizer or CNF was required to ensure adequate film formation.[15] Full gelatinization of AP prior to film casting may have been helpful in the present case, or higher molar mass. The average molar mass of AP is quite high ($M_n = 6.8 \times 10^7$) as is reported in SI (Table S1).

The most important observation from Figure 6a,b is that the Neat CNF membrane completely dominates the properties of the Core−shell CNF/AP nanocomposites. Young's modulus, yield strength, and tensile strength and strain to failure are very similar to data for Neat CNF, even for compositions with 23 wt % AP. As the relative humidity is increased to 85%, Core−shell CNF/AP still preserve the mechanical properties of Neat CNF. The compositions with 15 and 18 wt % AP show even better properties than Neat CNF, although part of the reason may be reduced porosity. It is still remarkable that, when present as a nanofiber coating, a polymer such as AP does not reduce the material properties.

The behavior of "Mixed" CNF/AP is very different. This nanocomposite displays substantial reduction in properties with increased AP matrix content, see Figure 6c,d. The "Mixed" CNF/AP composition with 25 wt % AP is directly comparable with the Core−shell CNF/AP 23 wt %. At 50% RH the comparison for "Mixed" versus Core−shell is Young's modulus 11.0 versus 13.6 GPa, yield strength 90.2 versus 117 MPa, and tensile strength 172 versus 221 MPa. At 85% RH the corresponding data are Young's modulus 8.64 versus 10.8 GPa, yield strength 50.3 versus 69.2 MPa, and tensile strength 99.6 versus 151 MPa. This is a strong effect since the materials have the same composition and the same CNF reinforcement, and primarily differ in the distribution of AP polymer matrix (see Figure 7). For Core−shell CNF/AP nanocomposites, the material consists of discrete nanofibers coated by AP polymer. The AP matrix is confined between CNF fibrils. The "unbound" AP present in the "Mixed CNF/AP", but not in Core−shell CNF/AP, has a role in the reduction of properties. The distribution of AP matrix in "Mixed" nanocomposite is much more inhomogeneous, possibly there are also AP-rich regions at the microscale. It means CNF−CNF interaction is more common, see Figure 7.

In Figure 6, it is notable that the mechanical properties of the Neat AP are favorable. This polymer often require additives in the form of plasticizers or CNF to overcome its brittleness.[15] Furthermore, the preparation procedure for "Mixed" CNF/AP included careful mixing. Still, the small scale differences in AP polymer matrix distribution are causing inferior properties to "Mixed" CNF/AP, as is apparent in Figure 6.

From the stress−strain curves in Figure 6, the "Mixed" CNF/AP shows nonlinear stress−strain behavior at much lower stress and strain than Core−shell CNF or Neat CNF. This observation is significant, since it indicates that the presence

DOI: 10.1021/bm5018194
Biomacromolecules 2015, 16, 904−912

of "unbound" AP significantly lowers the yield strength under moist conditions. Since strain-hardening then takes place at lowered stress level, this also leads to lowered tensile strength compared with Core−shell CNF/AP and Neat CNF.

In Core−shell CNF/AP, the strain hardening region[6] follows the same slope as for the Neat CNF. The network of CNF nanofibers deforms in a similar way and as efficiently as in the Neat CNF during plastic deformation. However, in "Mixed" CNF/AP the strain-hardening slope is lower, which means that the details of plastic deformation mechanisms are different.

Data from dynamic mechanical analysis performed at different relative humidities are presented in SI (Figure S7). The moisture-induced softening of "Mixed" CNF/AP occurred at much lower RH than for Core−shell CNF/AP. The thermal softening associated with polymer matrix T_g is shifted to much higher temperature as CNF is added to AP, see SI (Figure S8). This may be associated with reduced molecular mobility of the AP due to the proximity of more rigid CNF nanofibers.

CONCLUSIONS

Core−shell nanofibers are prepared, where CNF is the core and the AP polymer is associated with the CNF in the form of a thin "shell" coating. By the core−shell approach, the distribution of the polymer matrix is much better controlled than for conventional mixing of CNF with the dissolved polymer matrix. High fiber volume fractions can be achieved without loss of added polymer. AP promotes good CNF dispersion, possibly through steric hindrance effects from AP branches acting as polymer brushes.

Hygromechanical properties are exceptionally good, and much superior to "Mixed" CNF/AP, and any comparable cellulose/starch biocomposite material in the literature. For Core−shell CNF/AP 23 wt %, the modulus is 13.6 GPa, yield strength 117 MPa, ultimate strength 221 MPa and strain to failure 8%. The reduction in properties at 85%RH is much lower than expected for an AP composite.

The distribution of the AP as thin CNF coatings causes AP confinement as an interphase region next to rigid CNF nanofibers. This appears to restrict molecular mobility and hygroscopicity of AP, as indicated by low moisture sorption and comparably low sensitivity of mechanical properties to moist environment. Core−shell CNF nanocomposites are suitable for continuous papermaking-like processing of cellulose nanocomposites, a concept which could potentially be used industrially.

ASSOCIATED CONTENT

Supporting Information

Molecular weight analysis of AP, kinetic adsorption of AP on CNF, XRD measurement of CNF, AP, and Core−shell CNF/AP films, density and porosity measurement, observation of tensile fracture surface, a schematic model of core−shell nanofibers, moisture sorption data of Core−shell CNF/AP and "Mixed" CNF/AP compared with predicted values based on rule of mixture, tensile property data, and dynamic mechanical analysis (DMA) with humidity scanning. This material is available free of charge via the Internet at http://pubs.acs.org.

AUTHOR INFORMATION

Corresponding Author

*Phone: +46-8-790 81 18. E-mail: blund@kth.se.

Notes

The authors declare no competing financial interest.

ACKNOWLEDGMENTS

Wallenberg Wood Science Centre (WWSC) is gratefully acknowledged for providing lab facilities. Assoc. Prof. Qi Zhou is acknowledged for his suggestions for the adsorption study. Prof. Lars Wågberg is acknowledged for valuable comments. Anne-Mari Olsson is acknowledged for performing the DVS measurement at Innventia. Dr. Francisco Vilaplana is acknowledged for his help with SEC-MALLS measurements and AP data analysis.

REFERENCES

(1) Narayan, R. *MRS Bull.* **2011**, *36*, 716−721.
(2) Glasser, W. G. Cellulose and Associated Heteropolysaccharides. In *Glycoscience*; Fraser-Reid, B., Tatsuta, K., Thiem, J., Eds.; Springer: Berlin; Heidelberg, 2008; pp 1473−1512.
(3) Eichhorn, S. J.; Dufresne, A.; Aranguren, M.; Marcovich, N. E.; Capadona, J. R.; Rowan, S. J.; Weder, C.; Thielemans, W.; Roman, M.; Renneckar, S.; Gindl, W.; Veigel, S.; Keckes, J.; Yano, H.; Abe, K.; Nogi, M.; Nakagaito, A. N.; Mangalam, A.; Simonsen, J.; Benight, A. S.; Bismarck, A.; Berglund, L. A.; Peijs, T. *J. Mater. Sci.* **2009**, *45*, 1−33.
(4) Berglund, L. A.; Peijs, T. *MRS Bull.* **2010**, *35*, 201−207.
(5) Klemm, D.; Kramer, F.; Moritz, S.; Lindstrom, T.; Ankerfors, M.; Gray, D.; Dorris, A. *Angew. Chem., Int. Ed.* **2011**, *50*, 5438−5466.
(6) Henriksson, M.; Berglund, L. A.; Isaksson, P.; Lindström, T.; Nishino, T. *Biomacromolecules* **2008**, *9*, 1579−1585.
(7) Sehaqui, H.; Morimune, S.; Nishino, T.; Berglund, L. A. *Biomacromolecules* **2012**, *13*, 3661−3667.
(8) Sehaqui, H.; Zhou, Q.; Ikkala, O.; Berglund, L. A. *Biomacromolecules* **2011**, *12*, 3638−3644.
(9) Svagan, A. J.; Samir, M. A. S. A.; Berglund, L. A. *Adv. Mater.* **2008**, *20*, 1263−1269.
(10) Nakagaito, A. N.; Yano, H. *Appl. Phys. A: Mater. Sci. Process.* **2004**, *78*, 547−552.
(11) Pääkkö, M.; Vapaavuori, J.; Silvennoinen, R.; Kosonen, H.; Ankerfors, M.; Lindström, T.; Berglund, L. A.; Ikkala, O. *Soft Matter* **2008**, *4*, 2492−2499.
(12) Sehaqui, H.; Liu, A.; Zhou, Q.; Berglund, L. A. *Biomacromolecules* **2010**, *11*, 2195−2198.
(13) Wu, C. N.; Saito, T.; Fujisawa, S.; Fukuzumi, H.; Isogai, A. *Biomacromolecules* **2012**, *13*, 1927−1932.
(14) Abe, K.; Yano, H. *Carbohydr. Polym.* **2011**, *85*, 733−737.
(15) López-Rubio, A.; Lagaron, J. M.; Ankerfors, M.; Lindström, T.; Nordqvist, D.; Mattozzi, A.; Hedenqvist, M. S. *Carbohydr. Polym.* **2007**, *68*, 718−727.
(16) Svagan, A. J.; Hedenqvist, M. S.; Berglund, L. A. *Compos. Sci. Technol.* **2009**, *69*, 500−506.
(17) Svagan, A. J.; Samir, M. A. S. A.; Berglund, L. A. *Biomacromolecules* **2007**, *8*, 2556−2563.
(18) Zimmermann, T.; Bordeanu, N.; Strub, E. *Carbohydr. Polym.* **2010**, *79*, 1086−1093.
(19) Plackett, D.; Anturi, H.; Hedenqvist, M.; Ankerfors, M.; Gällstedt, M.; Lindström, T.; Siró, I. *J. Appl. Polym. Sci.* **2010**, 3601−3609.
(20) Dufresne, A.; Dupeyre, D.; Vignon, M. R. *J. Appl. Polym. Sci.* **2000**, *76*, 2080−2092.
(21) Dufresne, A.; Vignon, M. R. *Macromolecules* **1998**, *31*, 2693−2696.
(22) Angles, M. N.; Dufresne, A. *Macromolecules* **2001**, *34*, 2921−2931.
(23) Rindlav-Westling, Å.; Stading, M.; Hermansson, A.-M.; Gatenholm, P. *Carbohydr. Polym.* **1998**, *36*, 217−224.
(24) Pérez-Gallardo, A.; Bello-Pérez, L. A.; García-Almendárez, B.; Montejano-Gaitán, G.; Barbosa-Cánovas, G.; Regalado, C. *Starch/Stärke* **2012**, *64*, 27−36.

DOI: 10.1021/bm5018194
Biomacromolecules 2015, 16, 904−912

(25) Cobut, A.; Sehaqui, H.; Berglund, L. A. *Bioresource* **2014**, *9*, 3276−3289.
(26) Stading, M.; Rindlav-Westling, Å.; Gatenholm, P. *Carbohydr. Polym.* **2001**, *45*, 209−217.
(27) Ansari, F.; Galland, S.; Johansson, M.; Plummer, C. J. G.; Berglund, L. A. *Composites, Part A* **2014**, *63*, 35−44.
(28) Cosgrove, D. J. *Nat. Rev. Mol. Cell Biol.* **2005**, *6*, 850−61.
(29) Whitney, S. E. C.; Gothard, M. G. E.; Mitchell, J. T.; Gidley, M. J. *Plant Physiol.* **1999**, *121*, 657−663.
(30) Carpita, N. C.; McCann, M. C.The Cell Wall. In *Biochemistry and Molecular Biology of Plants*; Buchanan, B. B., Gruissem, W., Jones, R., Eds.; American Society Plant Physiologists: Rockville, MD, 2000; Chapter 2.
(31) Awano, T.; Takabe, K.; Fujita, M.; Daniel, G. *Protoplasma* **2000**, *212*, 72−79.
(32) Zhou, Q.; Malm, E.; Nilsson, H.; Larsson, P. T.; Iversen, T.; Berglund, L. A.; Bulone, V. *Soft Matter* **2009**, *5*, 4124−4130.
(33) Sehaqui, H.; Zhou, Q.; Berglund, L. A. *Soft Matter* **2011**, *7*, 7342−7350.
(34) Ahola, S.; Österberg, M.; Laine, J. *Cellulose* **2007**, *15*, 303−314.
(35) Stevanic, J. S.; Mikkonen, K. S.; Xu, C.; Tenkanen, M.; Berglund, L.; Salmén, L. *J. Mater. Sci.* **2014**, *49*, 5043−5055.
(36) Henriksson, M.; Henriksson, G.; Berglund, L. A.; Lindström, T. *Eur. Polym. J.* **2007**, *43*, 3434−3441.
(37) Svagan, A. J.; Azizi Samir, M. A. S.; Berglund, L. A. *Biomacromolecules* **2007**, *8*, 2556−2563.
(38) Evans, D. F.; Wennerström, H. *The Colloidal Domain: Where Physics, Chemistry, Biology, and Technology Meet (Advances in Interfacial Engineering)*, 2nd ed.; Wiley-VCH Verlag GmbH: New York, 1999.
(39) Olszewska, A.; Junka, K.; Nordgren, N.; Laine, J.; Rutland, M. W.; Österberg, M. *Soft Matter* **2013**, *9*, 7448−7457.
(40) Olszewska, A.; Valle-Delgado, J. J.; Nikinmaa, M.; Laine, J.; Osterberg, M. *Nanoscale* **2013**, *5*, 11837−11844.
(41) Lucenius, J.; Parikka, K.; Österberg, M. *React. Funct. Polym.* **2014**, *85*, 167−174.
(42) Somasundaran, P.; Mehta, S. C.; Yu, X.; Krishnakumar, S. *Handbook of Surface and Colloid Chemisty: Colloid Systems and Interfaces Stability of Dispersions through Polymer and Surfactant Adsorption*, 3rd ed.; Taylor & Francis Group, LLC: Oxford, U.K., 2009.
(43) Lowell, S.; Shields, J. E.; Thomas, M. A.; Thommes, M. *Characterization of Porous Solids and Powders: Surface Area, Pore Size, and Density*; Kluwer Academic Publishers: Norwell, MA, 2004; p 349.
(44) Engelund, E. T.; Thygesen, L. G.; Svensson, S.; Hill, C. A. S. *Wood Sci. Technol.* **2013**, *47*, 141−161.

DOI: 10.1021/bm5018194
Biomacromolecules 2015, 16, 904−912